Molecular corridors and kinetic regimes in the multiphase chemical evolution of secondary organic aerosol

M. Shiraiwa[1], T. Berkemeier[1], K. A. Schilling-Fahnestock[2], J. H. Seinfeld[2], and U. Pöschl[1]

[1]Multiphase Chemistry Department, Max Planck Institute for Chemistry, 55128 Mainz, Germany
[2]Division of Chemistry and Chemical Engineering, California Institute of Technology, Pasadena, CA 91125, USA

Correspondence to: M. Shiraiwa (m.shiraiwa@mpic.de)

Abstract. The dominant component of atmospheric, organic aerosol is that derived from the oxidation of volatile organic compounds (VOCs), so-called secondary organic aerosol (SOA). SOA consists of a multitude of organic compounds, only a small fraction of which has historically been identified. Formation and evolution of SOA is a complex process involving coupled chemical reaction and mass transport in the gas and particle phases. Current SOA models do not embody the full spectrum of reaction and transport processes, nor do they identify the dominant rate-limiting steps in SOA formation. Based on molecular identification of SOA oxidation products, we show here that the chemical evolution of SOA from a variety of VOC precursors adheres to characteristic "molecular corridors" with a tight inverse correlation between volatility and molar mass. The slope of these corridors corresponds to the increase in molar mass required to decrease volatility by one order of magnitude ($-\mathrm{d}M / \mathrm{dlog}C_0$). It varies in the range of 10–30 g mol^{-1}, depending on the molecular size of the SOA precursor and the O : C ratio of the reaction products. Sequential and parallel reaction pathways of oxidation and dimerization or oligomerization progressing along these corridors pass through characteristic regimes of reaction-, diffusion-, or accommodation-limited multiphase chemical kinetics that can be classified according to reaction location, degree of saturation, and extent of heterogeneity of gas and particle phases. The molecular corridors and kinetic regimes help to constrain and describe the properties of the products, pathways, and rates of SOA evolution, thereby facilitating the further development of aerosol models for air quality and climate.

1 Introduction

Organic aerosol is ubiquitous in the atmosphere and its major component is secondary organic aerosol (SOA) (Jimenez et al., 2009). Reaction of atmospheric volatile organic compounds (VOCs) with oxidants such as OH, O$_3$, and NO$_3$ initiate the formation of semi-volatile organic compounds (SVOCs), which can undergo further gas-phase oxidation to form low-volatility organic compounds (LVOCs) that will preferentially partition into the particle phase (Kroll and Seinfeld, 2008; Hallquist et al., 2009; Donahue et al., 2012; Murphy et al., 2014). A fraction of the SVOCs partitions into the particle phase, wherein they can be transformed into LVOCs such as dimers, oligomers, and other high molecular mass compounds (Jang et al., 2002; Kalberer et al., 2006; Ervens et al., 2011; Ziemann and Atkinson, 2012; Shiraiwa et al., 2013a). Some portion of the LVOCs can be transformed back to (semi-)volatile compounds or CO / CO$_2$ by fragmentation reactions triggered by OH or other oxidants at the particle surface or in the particle bulk (Bertram et al., 2001; Kroll and Seinfeld, 2008; Jimenez et al., 2009). SOA partitioning is also affected by particle-phase state, non-ideal thermodynamic mixing, and morphology (Chang and Pankow, 2006; Zuend and Seinfeld, 2012; Shiraiwa et al., 2013b).

SOA consists of a myriad of organic compounds, of which only 10–30 % have been identified (Goldstein and Galbally, 2007). Common techniques applied for the analysis of SOA are gas chromatography/electron impact ionization mass spectrometry (GC/EI-MS) and liquid chromatography/electrospray ionization mass spectrometry (LC/ESI-MS) (e.g., Surratt et al., 2006). Hard ionization, such as electron impact ionization, generally causes significant fragmentation

of organic molecules, which makes molecular identification challenging, but can provide molecular structural information. The recent advent of soft ionization methods such as electrospray ionization (ESI), matrix-assisted laser desorption ionization (MALDI), atmospheric pressure chemical ionization (APCI), and direct analysis in real time (DART) ionization has facilitated the identification of the dominant fraction of the compounds constituting SOA by preserving analytes as intact or nearly intact during ionization (Kalberer et al., 2006; Williams et al., 2010; Laskin et al., 2012a, b; Chan et al., 2013; Nguyen et al., 2013; Vogel et al., 2013; Schilling-Fahnestock et al., 2014). Taking advantage of such data, here we present a new, 2-D map for SOA evolution of molar mass vs. volatility, which can be linked to kinetic regimes and reaction pathways of formation and aging of SOA that is currently poorly constrained and a major limitation in the understanding and prediction of atmospheric aerosol effects.

2 Molecular corridors for different SOA precursors

Figure 1 shows 2-D maps of molecular weight or molar mass (M) plotted against volatility or saturation mass concentration (C_0) for organic compounds in SOA from a range of anthropogenic and biogenic precursors: dodecane (Fig. 1a, b) (Yee et al., 2012), cyclododecane (Fig. 1c, d), hexylcyclohexane (Fig. 1e, f) (Schilling-Fahnestock et al., 2014), α-pinene (Fig. 1g) (Docherty et al., 2005; Claeys et al., 2007, 2009; Zuend and Seinfeld, 2012; Kahnt et al., 2014; Kristensen et al., 2014), limonene (Fig. 1h) (Jaoui et al., 2006; Kundu et al., 2012), isoprene (Fig. 1i) (Surratt et al., 2006; Surratt et al., 2010; Lin et al., 2012, 2013), glyoxal and methylglyoxal (Fig. 1j) (Lim et al., 2010; Sareen et al., 2010; Zhao et al., 2012). Experimental conditions including oxidants, NO levels, and seed particles used in earlier studies are summarized in Table A1. The experimental conditions and methods applied in this study to analyze the formation and composition of SOA from C_{12} alkanes under low and high NO conditions are detailed in Appendix A and Schilling-Fahnestock et al. (2014). DART is a soft ionization technique of atmospheric pressure ionization that has recently been used for the analysis of a variety of organic compounds with minimal fragmentation (Chan et al., 2013). SOA compounds identified include alcohols, ketones, aldehydes, hydroxycarbonyls, organic hydroperoxides, and nitrates, which are generated in the gas phase (open markers), as well as dihydrofuran, furan, ether, ester, peroxyhemiacetal, hemiacetal, dimer, and imine, which are likely particle-phase products (Ziemann and Atkinson, 2012) (solid markers). Through the combination of an aerosol mass spectrometer (AMS) and DART-MS, close to 100 % identification and quantification of the particle phase for each of the three alkane systems was achieved (Schilling-Fahnestock et al., 2014). Thus, alkane SOA are plotted for low and high NO conditions in separate panels due to large

number of identified products, whereas biogenic SOA data are shown in one panel due to the relatively small number of data points.

Vapor pressures and saturation mass concentrations of organic compounds were estimated using the "estimation of vapor pressure of organics, accounting for temperature, intramolecular, and non-additivity effects" (EVAPORATION) model, (Compernolle et al., 2011). The EVAPORATION model estimates vapor pressure of molecules with the following functionalities: aldehyde, ketone, alcohol, ether, ester, nitrate, acid, peroxide, hydroperoxide, peroxy acyl nitrate, and peracid. Organosulfates and imidazoles are not covered and were thus not included in our analysis, although they have been identified in SOA from biogenic precursors and glyoxal (Iinuma et al., 2007; Surratt et al., 2008; Ervens et al., 2011).

The markers in Fig. 1 are color-coded with atomic O : C ratio. Generally, volatility decreases and molar mass increases with chemical aging of SOA both in the gas and particle phases. Consequently, molar mass of oxidation products tightly correlates with volatility with high coefficient of determination (R^2), as summarized in Table 1. The 95 % prediction intervals (dashed lines in Fig. 1) can be regarded as molecular corridors, within which additional unidentified oxidation products are likely to fall. The negative slope of the fit lines corresponds to the increase in molar mass required to decrease volatility by one order of magnitude, $-\mathrm{d}M / \mathrm{dlog}C_0$. It increases from $\sim 10\,\mathrm{g\,mol^{-1}}$ for glyoxal, and methylglyoxal to $\sim 25\,\mathrm{g\,mol^{-1}}$ for dodecane and cyclododecane, depending on the molecular size of the SOA precursor and the O : C ratio of the reaction products, as will be discussed below. The mean value of $-\mathrm{d}M / \mathrm{dlog}C_0$ average over all investigated systems is $20 \pm 4\,\mathrm{g\,mol^{-1}}$.

The composition of SOA may vary depending not only on the organic precursor, but also on the oxidant and other reaction conditions of formation and aging (Presto et al., 2005; Surratt et al., 2006; Lin et al., 2012, 2013; Kristensen et al., 2014; Loza et al., 2014; Xu et al., 2014). The atomic O : C ratio tends to be higher at high NO concentrations, partly due to the formation of organonitrates (Nguyen et al., 2011; Schilling-Fahnestock et al., 2014). Even though Fig. 1g, h, and i contain biogenic SOA oxidation products measured under different conditions, as specified in Table A1, the molecular corridors are relatively tight with $R^2 > 0.85$. The molecular corridors of alkane SOA formed under low and high NO conditions are also quite similar (Fig. 1a–f). Thus, the molecular corridors of SOA formation appear to be determined primarily by the organic precursor, and the extent to which they are influenced by reaction conditions warrants further studies.

3 Kinetic regimes and limiting cases

Traditionally, SOA formation has been modeled based on instantaneous gas-particle equilibrium partitioning, implicitly
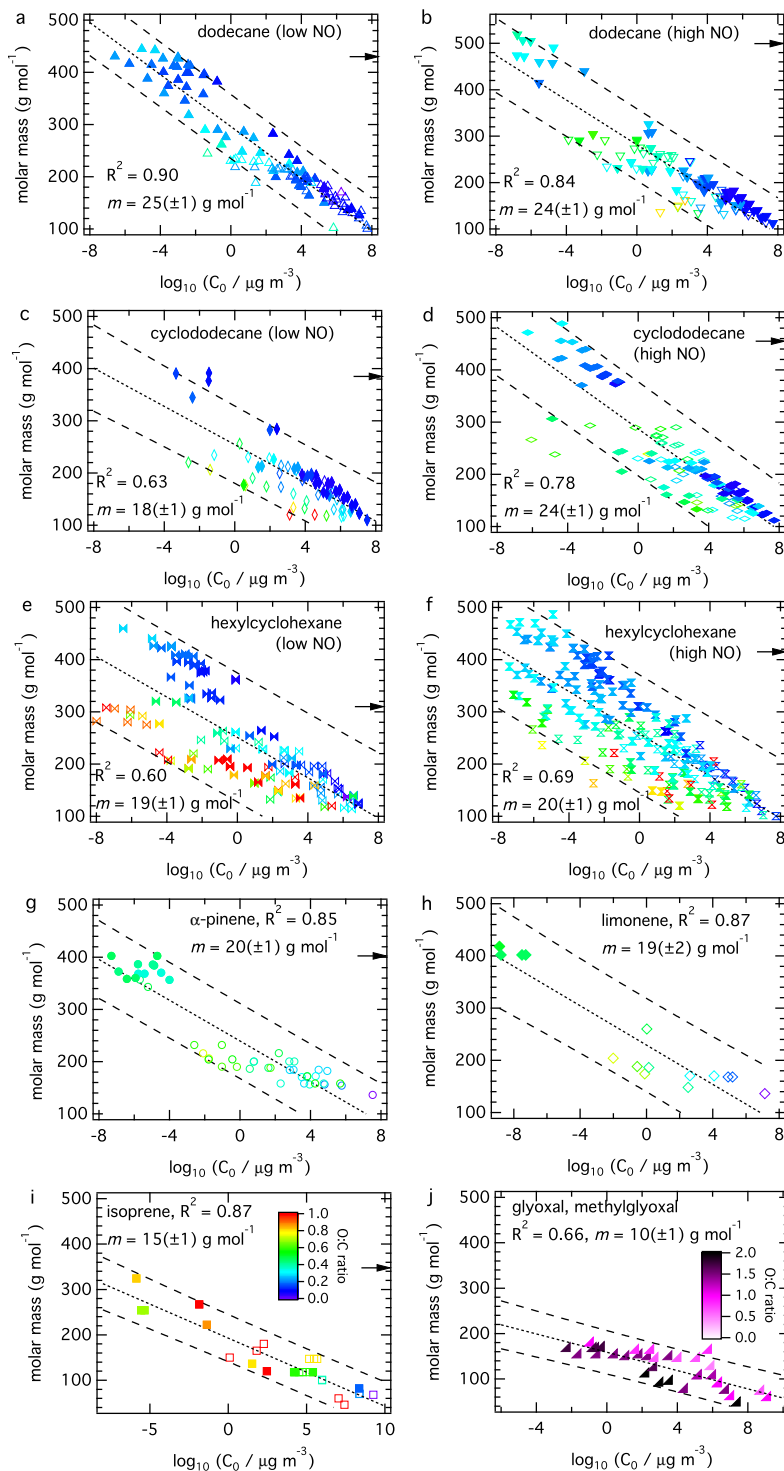
Figure 1. Molecular corridors of SOA evolution for different precursor compounds. Molar mass vs. volatility (saturation mass concentration, C_0) at 298 K for oxidation products of dodecane at **(a)** low and **(b)** high NO condition, cyclododecane at **(c)** low and **(d)** high NO condition, and hexylcyclohexane at **(e)** low and **(f)** high NO condition and **(g)** α-pinene, **(h)** limonene, **(i)** isoprene, and **(j)** glyoxal and methylglyoxal. The open and solid markers correspond to the gas- and particle-phase products, respectively, color-coded by atomic O : C ratio (note different color scale for **j**). With a linear regression analysis, the coefficient of determination (R^2), fitted lines (dotted lines) and their slopes (m), and prediction intervals with 95 % confidence (dashed lines) are shown. The arrows on the right axis indicate average molar mass for isoprene and α-pinene (Kalberer et al., 2006), as well as for alkanes, as measured in this study.

Table 1. Summary of analysis of identified SOA oxidation products. Number of identified oxidation products N, average molar mass M_{ave}, negative slope ($-dM / d\log C_0$) of fitted lines in Fig. 2 of molar mass vs. logarithm of volatility, coefficients of determination R^2, as well as R^2 for O : C vs. logarithm of volatility.

| Precursor	N	M_{ave} (g mol^{-1})	$-dM / d\log C_0$ (g mol^{-1})	R^2 (molar mass)	R^2 (O : C)
Dodecane, low NO	116	429	25(± 1)	0.90	0.22
Dodecane, high NO	106	495	24(± 1)	0.84	0.29
Cyclododecane, low NO	77	384	18(± 1)	0.63	0.08
Cyclododecane, high NO	122	458	24(± 1)	0.78	0.08
Hexylcyclohexane, low NO	137	310	19(± 1)	0.60	0.05
Hexylcyclohexane, high NO	230	418	20(± 1)	0.69	0.00
α-pinene	47	400*	20(± 1)	0.85	0.13
Limonene	17	–	19(± 2)	0.87	0.38
Isoprene	29	350*	15(± 1)	0.87	0.09
Glyoxal, methylglyoxal	35	-	10(± 1)	0.66	0.16

* Kalberer et al. (2006).
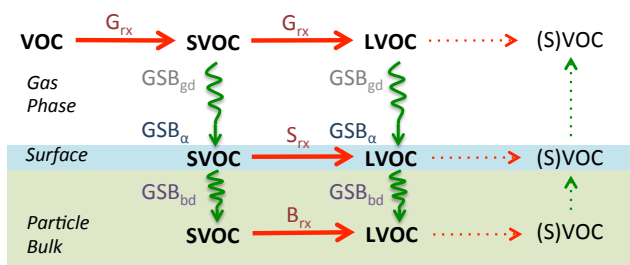
Figure 2. Molecular processes of SOA evolution: schematic outline of formation and aging. Red and green arrows denote chemical reactions and mass transport, respectively. Sequential and parallel reactions in the gas phase, at the particle surface, and in the particle bulk lead to multiple generations of volatile, semi-volatile and low-volatile organic compounds (VOC, SVOC, LVOC). Dotted arrows denote revolatilization resulting from fragmentation reactions. Labels on arrows relate to kinetic regimes outlined in subsequent figure.

assuming that gas-phase reactions are the rate-limiting step of SOA formation and growth (Pankow, 1994; Donahue et al., 2006; Hallquist et al., 2009). Recent studies, however, have shown that mass transport and chemical reaction in the particle phase may also play an important role (Fig. 2) (Ervens et al., 2011; Ziemann and Atkinson, 2012; Shiraiwa et al., 2013a). Recently, Berkemeier et al. (2013) provided a conceptual framework which enables the characterization of heterogeneous reactions and gas uptake in atmospheric aerosols and clouds through a well-defined set of distinct kinetic regimes and limiting cases. We extended this framework to cover the complex interplay of gas- and particle-phase reactions in the evolution of SOA and to enable a systematic classification of rate-limiting processes in the analysis and interpretation of laboratory chamber data and ambient measurements, as well as in the comparison of experimental results with theoretical predictions.

Different types of kinetic behavior can be characterized by three basic criteria as detailed in the Appendix B: (1) the location of the chemical reaction leading to SOA formation or aging (gas phase, particle surface, particle bulk); (2) the saturation ratio of the reactants (ratio of ambient concentration to saturation concentration); and (3) the extent of spatial heterogeneity of the gas and particle phases (concentration gradients). The kinetic regimes and limiting cases defined by these criteria can be visualized on a "kinetic cuboid", in which each axis corresponds to one of the three classification parameters, as shown in Fig. 3a. The symbols "G", "S", and "B" indicate the predominant reaction location: gas phase, particle surface, or particle bulk, respectively. A subscript denotes the rate-limiting process for SOA formation and aging: "rx" indicates chemical reaction; "bd" indicates bulk diffusion; "α" indicates mass accommodation; "gd" indicates gas-phase diffusion. Depending on atmospheric composition and reaction conditions, which vary widely in space and time, the chemical evolution of organic compounds and SOA particles can progress through any of these regimes.

The left part of the cuboid can be regarded as a particle-phase chemistry regime, and the right side as a gas-phase chemistry regime. As shown in Fig. 3b, the particle-phase chemistry regime (SB, including surface (S) or bulk (B) reaction) can be further subdivided into a reaction-diffusion regime (SBrd), where the system is limited by reaction or diffusion in the particle-phase, and a mass-transfer regime (SB^{mt}) limited by mass accommodation at the interface or diffusion through the gas phase (Berkemeier et al., 2013). The gas-phase chemistry regime (G) comprises the traditional scenario of SOA formation determined by a rate-limiting chemical reaction in the gas phase, followed by quasi-instantaneous gas-particle partitioning of the reaction products (G$_{rx}$), corresponding to so-called quasi-equilibrium growth (Shiraiwa and Seinfeld, 2012; Zhang et al., 2012). The rest of the gas-phase chemistry regime is mass transport-limited and corresponds to so-called non-equilibrium growth
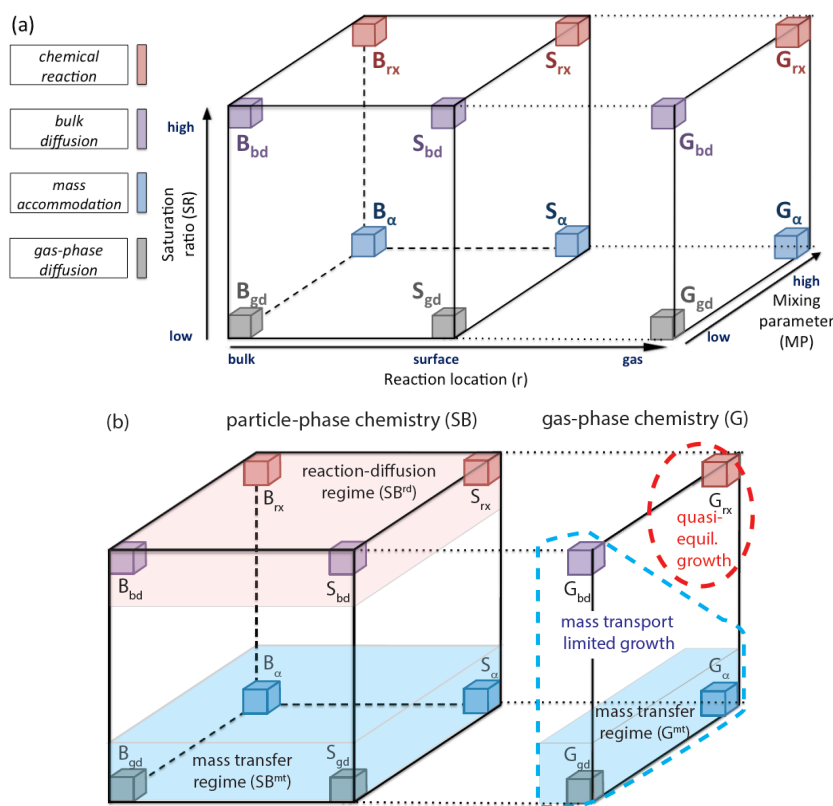
Figure 3. Kinetic regimes and limiting cases of SOA evolution mapped onto the axes of a cuboid representing reaction location, saturation ratio, and mixing parameter. **(a)** Horizontal edges of the cuboid (left to right) correspond to four regimes governed by chemical reaction ("rx", red), bulk diffusion ("bd", purple), mass accommodation ("α", blue), or gas-phase diffusion ("gd", grey). Each of these regimes includes three distinct limiting cases characterized by a single rate-limiting process and a dominant reaction location (particle bulk, B; surface, S; gas phase, G). **(b)** The left side of the cuboid can be regarded as a particle-phase chemistry regime (SB) and subdivided into a reaction-diffusion regime (SBrd) and a mass transfer regime (SB^{mt}). The right side of the cuboid can be regarded as a gas-phase chemistry regime (G) and subdivided into a traditional scenario of "quasi-equilibrium growth", limited only by a gas phase reaction, followed by quasi-instantaneous gas-particle partitioning (G$_{rx}$) and a mass-transport limited regime of "non-equilibrium growth" that may be kinetically limited by gas-to-particle mass transfer (G^{mt}) or diffusion in the particle (G$_{bd}$).

(Perraud et al., 2012; Zaveri et al., 2014), which can be kinetically limited by gas-to-particle mass transfer (gas-phase diffusion and accommodation at the interface; G^{mt}) or retarded diffusion in the particle phase (G$_{bd}$).

4 Characteristic pathways and properties

Figure 4a shows the ensemble of molecular corridors from Fig. 1 with a total of 909 identified oxidation products from seven different SOA precursors. They are constrained by two boundary lines corresponding to the volatility of n-alkanes C_nH_{2n+2} and sugar alcohols $C_nH_{2n+2}O_n$. These lines illustrate the regular dependence of volatility on the molar mass of organic compounds; the different slopes of 30 g mol^{-1} for C_nH_{2n+2} and 12 g mol^{-1} for $C_nH_{2n+2}O_n$ reflect that the decrease of volatility with increasing molar mass is stronger for polar compounds (see Fig. D2 for alternative representation).

Many early generation gas-phase oxidation products of alkanes, as well as dimers or oligomers with low O : C ratio (LOC), fall into a molecular corridor close to the C_nH_{2n+2} line, which we designate as LOC corridor ($-dM / dlogC_0 \geq \sim 25$ g mol^{-1}, blue shaded area). Aqueous-phase reaction and autoxidation products with high O : C ratio (HOC), on the other hand, tend to fall into a corridor near the $C_nH_{2n+2}O_n$ line, which we designate as HOC corridor ($-dM / dlogC_0$ of $\leq \sim 15$ g mol^{-1}, red shaded area). The area in between is characterized by intermediate O : C ratios and accordingly designated as IOC corridor ($-dM / dlogC_0 \approx \sim 20$ g mol^{-1}). Among the SOA systems investigated in this study, the small precursor VOCs glyoxal, methylglyoxal, and isoprene (C_2–C_5) evolve through the HOC corridor, and the terpenes α-pinene and limonene (C_{10}) through the IOC corridor. The alkanes dodecane and cyclododecane (C_{12}) evolve through the LOC corridor, while hexylcyclohexane exhibits a branching between the LOC and
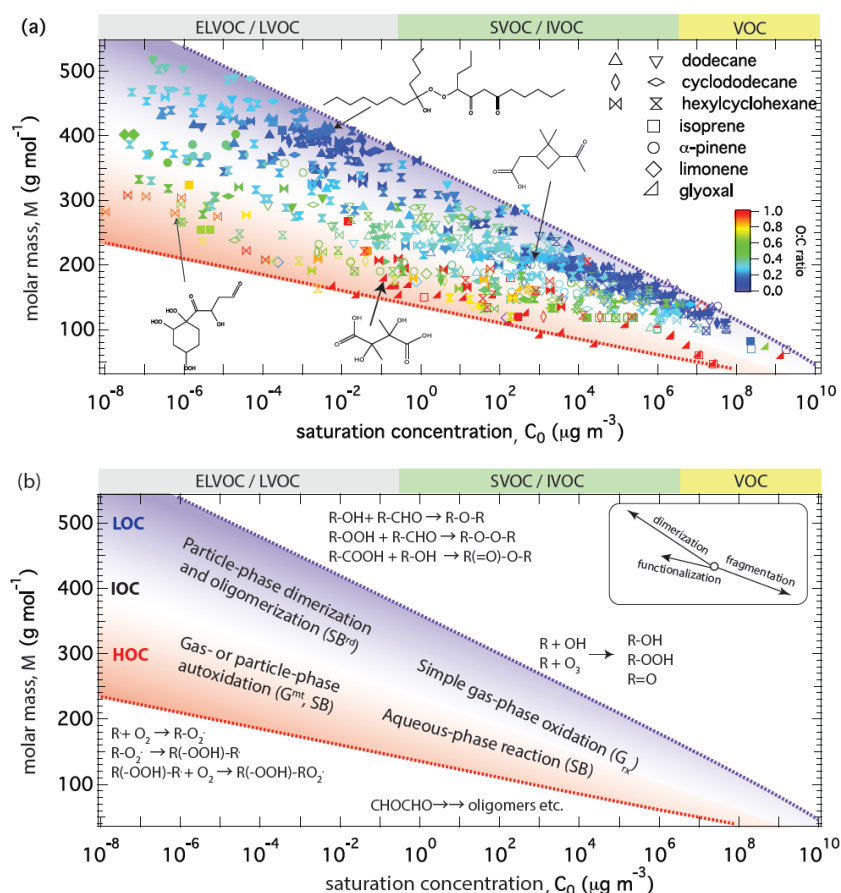
Figure 4. Ensemble of molecular corridors and kinetic regimes of SOA evolution. **(a)** Molar mass vs. volatility (C_0) at 298 K for gas-phase (open) and particle-phase (solid) oxidation products of anthropogenic precursors (dodecane, cyclododecane, hexylcyclohexane) under low/high NO conditions, biogenic precursors (α-pinene, limonene, isoprene) and aqueous-phase reaction products of glyoxal and methylglyoxal. The dotted lines represent linear alkanes C_nH_{2n+2} (purple with O : C = 0) and sugar alcohols $C_nH_{2n+2}O_n$ (red with O : C = 1). Chemical structures of some representative products are shown. **(b)** Characteristic reaction pathways with most probable kinetic regimes. Molecular corridors consists of high, intermediate and low O : C corridors (HOC, red shaded area; IOC, white area; LOC, blue shaded area). SOA products evolve over the molecular corridor driven by three key reaction types of functionalization, oligomerization, and fragmentation, as illustrated in the insert (note different lengths of arrows indicating different intensities of effects on volatility).

HOC corridors, suggesting the involvement of different reaction pathways. For unidentified SOA products, the molecular corridor ensemble in Fig. 4a and alternative representations (Fig. D2a) may also be used as a look-up plot to obtain a rough estimate of volatility by comparison of molar mass and O : C ratio (e.g., from soft-ionization high-resolution mass spectrometry) to the data in the plot.

Characteristic reaction pathways and relevant kinetic regimes are outlined in Fig. 4b. SOA precursor VOCs with high volatility and low molar mass are located in the lower right corner of the molecular corridor ensemble. As illustrated in the insert in Fig. 4b, single-step functionalization usually leads to a small increase in molar mass, corresponding to one order of decrease in volatility (Donahue et al., 2006), while dimerization and oligomerization tend to multiply molar mass, and thus decrease volatility by multiple orders of magnitude (Trump and Donahue, 2014) (e.g., three

to four orders of magnitude for alkane and terpene SOA, see Fig. 1). Fragmentation, on the other hand, can lead to a substantial decrease of molar mass and increase in volatility (Bertram et al., 2001; Yee et al., 2012; Schilling-Fahnestock et al., 2014). As a result, simple gas-phase oxidation products are confined to the lower right area in the 2-D space. Such oxidation products ($C_0 > 10 \, \mu g \, m^{-3}$) tend to fall into the gas-phase reaction limiting case G_{rx} (quasi-equilibrium growth), as their gas-particle equilibration timescale is on the order of seconds to minutes (Shiraiwa and Seinfeld, 2012) (see Appendices C and D).

Particle-phase dimerization and oligomerization involving two or more molecules usually leads to the formation of compounds with low volatility and high molar mass lying in the upper left area in the 2-D space. The formation of such particle-phase products is likely limited by reaction or diffusion in the particle bulk (SB^{rd}), as rate coefficients for dimer
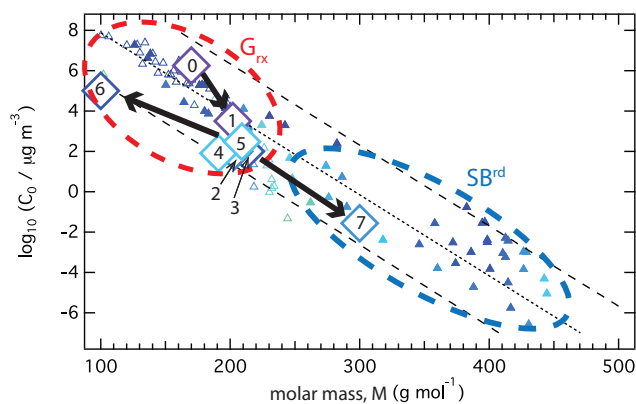
Figure 5. Evolution of reaction pathways over the molecular corridor of dodecane SOA under low NO condition. The large diamonds indicate the surrogate compounds used in the kinetic multi-layer model for gas-particle interactions (KM-GAP) simulations (Appendix D; Shiraiwa et al., 2013a), including the precursor (dodecane, 0), 1st–5th generations of surrogate products of gas-phase oxidation (1–5), gas-phase fragmentation (aldehydes, 6), and particle-phase dimerization products (7). The smaller symbols indicate identified individual products (as shown in Fig. 1a).

formation are relatively low ($< 10\,M^{-1}\,s^{-1}$) (Ziemann and Atkinson, 2012) and large molecules tend to diffuse slowly (Pfrang et al., 2011; Shiraiwa et al., 2011; Abramson et al., 2013; Zhou et al., 2013). An example of reaction pathways leading to dimerization is shown in Fig. 5 for dodecane SOA (Appendix D, Shiraiwa et al., 2013a). Within the molecular corridor of dodecane SOA evolution, Fig. 5 illustrates a specific trajectory from the precursor (dodecane, 0) through multiple generations of surrogate products of gas-phase oxidation and functionalization (multifunctional alcohols, ketones, and peroxides, 1–5), gas-phase fragmentation (aldehydes, 6), and particle-phase dimerization between aldehydes and peroxides to peroxyhemiacetals (7). Numerical model results shown in Figs. 5 and D1 indicate that the trajectory of chemical evolution passes through different kinetic regimes, i.e., from limitation by gas-phase reaction (G_{rx}) to particle-phase reaction and diffusion (SB^{rd}). Note that particle-phase reactions may also be limited by gas-to-particle mass transfer (e.g., accommodation, supply of reactive gases into the particle), when they are sufficiently fast, i.e., catalyzed by acids (Jang et al., 2002; Iinuma et al., 2004; Offenberg et al., 2009; Surratt et al., 2010).

Aqueous-phase processing of glyoxal and methylglyoxal is an efficient pathway for formation of low volatility and semi-volatile HOC compounds (Liggio et al., 2005; Carlton et al., 2007; Lim et al., 2010; Ervens et al., 2011; Zhao et al., 2012). Uptake of glyoxal into the particle phase leads to hydration and acid catalysis to form hemiacetals, aldols, imines, anhydrides, esters, and organosulfates (Lim et al., 2010). Reactive uptake of isoprene epoxydiols (IEPOX) and subsequent formation of oligomers (Surratt et al., 2010; Lin

et al., 2012, 2013) also progresses over the HOC corridor. Whether multiphase chemistry of glyoxal and IEPOX is limited by mass transfer or chemical reactions may depend on various factors including reaction rate coefficients, relative humidity, particle pH, and Henry's law constant (Ervens and Volkamer, 2010; McNeill et al., 2012; Kampf et al., 2013).

Recently, highly oxidized, extremely low volatility organic compounds (ELVOC) have been detected in field and chamber experiments (Ehn et al., 2012; Schobesberger et al., 2013; Ehn et al., 2014). Such compounds may populate the upper left corner of the HOC corridor. It has been shown that such compounds can be formed via autoxidation (inter- and intramolecular hydrogen abstraction by peroxy radicals) in the gas and particle phases (Crounse et al., 2013). When they are formed in the gas phase, the equilibration timescale of partitioning is long due to their low volatility, and the SOA growth is limited most likely by mass transfer (gas-phase diffusion and accommodation; G^{mt}) (see Appendix C and Fig. C1) (Pierce et al., 2011; Riipinen et al., 2011; Shiraiwa and Seinfeld, 2012). Note that kinetic limitation by retarded bulk diffusion (G_{bd}) is also possible for semi-volatile and low-volatility products when organic particles adopt amorphous, solid state (Virtanen et al., 2010; Cappa and Wilson, 2011; Shiraiwa et al., 2011; Vaden et al., 2011; Kuwata and Martin, 2012; Perraud et al., 2012; Shiraiwa and Seinfeld, 2012; Renbaum-Wolff et al., 2013; Zaveri et al., 2014). Indeed, recent observation found that some SVOCs do not necessarily adhere to equilibrium partitioning (Vogel et al., 2013).

Formation of high molecular weight SOA compounds from oligomerization or autoxidation results in high average molar mass for the biogenic systems of isoprene and α-pinene (Kalberer et al., 2006), as well as the anthropogenic C_{12} alkanes (Fig. 1 and Table 1; Schilling-Fahnestock et al., 2014). Figure 4a shows that most identified oxidation products with molar masses higher than $300\,g\,mol^{-1}$ are particle-phase products (solid markers). Thus, the relatively high average molar mass observed for laboratory-generated SOA points to the importance of particle-phase chemistry in these systems. Some SOA compounds with higher molar mass are gas-phase oxidation products including ELVOC and ester dimers observed in α-pinene oxidation (Ehn et al., 2014; Kristensen et al., 2014), and there are also some particle-phase products with relatively low molar mass, including furans and dihydrofurans in dodecane and cyclododecane SOA (Yee et al., 2012; Loza et al., 2014), as well as glyoxal and IEPOX products in isoprene SOA (Lim et al., 2010; Surratt et al., 2010). Nevertheless, the clustering of identified reaction products in molecular corridors may facilitate estimation of the relative importance of gas- vs. particle-phase routes to SOA formation (Fig. 1).

Molar mass and O : C ratio also correlate with the glass transition temperature of organic compounds, which tends to rise with increasing molar mass and O : C ratio (Koop et al., 2011). As elevated glass transition temperatures are indicative of semi-solid or amorphous, solid states, SOA evolution

represented in molecular corridors allows one to infer the regime in which particles are likely to become highly viscous. For example, recent experiments have shown an order of magnitude increase in the viscosity of oleic acid particles upon reaction with ozone owing to formation of oligomers (Hosny et al., 2013), and model calculations indicate that this may lead to the formation of surface crusts (Pfrang et al., 2011).

In summary, presenting identified SOA products in a molecular corridor encapsulates fundamental aspects of SOA formation and aging: volatility, molar mass, O : C ratio, and phase state. Such a representation can be used to constrain and/or predict the properties of unidentified SOA oxidation products. The kinetic regimes, within which SOA evolution is occurring along the molecular corridor, facilitate the specification of the rate of progression to higher generation products. Thus, molecular corridors may serve as a basis for compact representation of SOA formation and aging in regional and global models of climate and air quality.

Appendix A: Product analysis of alkane SOA

Photo-oxidation and subsequent SOA formation of *n*-dodecane, cyclododecane, and hexylcyclohexane was conducted in the $28\,m^3$ Teflon reactors in the Caltech environmental chamber (Yee et al., 2012; Loza et al., 2014; Schilling-Fahnestock et al., 2014). Aqueous H_2O_2 solution was evaporated into the chamber as the OH source, followed by the atomization of an aqueous ammonium sulfate solution generating seed particles, which were subsequently dried. Experiments were conducted under low NO conditions, in which alkyl peroxy radicals (RO_2) react primarily with HO_2, and under high NO conditions, in which RO_2 react primarily with NO (Loza et al., 2014).

SOA particles were collected on Teflon filters (Pall Life Sciences, 47 mm, $1.0\,\mu m$ pore size). Off-line analysis of collected particles was conducted by solvent extraction and gas chromatography time-of-flight mass spectrometry (GC-TOF-MS, GCT Premier, Waters) and GC / ion trap mass spectrometry (Varian Saturn 2000, Agilent), and by direct analysis in real time (DART) time-of-flight and ion trap mass spectrometry (DART-AccuToF, JEOL USA; Caltech Mini-DART; LTQ, Thermo Fisher). Further details on experimental conditions and analytical methods can be found in Schilling-Fahnestock et al. (2014).

The average molar mass of SOA was estimated by taking the sum of the product of the percent-relative concentration of each compound with respect to the internal standard (dibutyl phthalate present in each filter) by each compound's molar mass. The relative concentration for each compound was obtained through the relationship of ion current intensity and concentration for DART-MS. In DART analysis, ion current intensity (I) is proportional to the concentration (C), vapor pressure (P_{vap}) and proton affinity (A): $I = AP_{vap}C$. This equation is written for both the analyte and the internal standard and then the ratio is calculated, which allows for the cancellation of the proton affinity term. Analyte vapor pressures were estimated by using proposed structures based on HR-MS data-derived formulae and known mechanisms with the EVAPORATION model (Compernolle et al., 2011). When rewritten to solve for the relative concentration of the analyte with respect to the concentration of the internal standard, the equation becomes

$$\frac{C_A}{C_{IS}} = \frac{P_{vap,IS}}{P_{vap,A}} \cdot \frac{I_A}{I_{IS}}.$$

Atomic O : C ratio vs. volatility is used to represent formation and aging of SOA (Jimenez et al., 2009; Donahue et al., 2011). By analogy to Figs. 1 and 4, major oxidation products are shown in Figs. S1 and S2 in the Supplement. The markers are color-coded by molar mass. Upon gas-phase oxidation, volatility decreases and O : C ratio increases, leading to a linear correlation in O : C ratio vs. volatility for gas-phase oxidation products. Particle-phase products, however, exhibit generally lower volatility and O : C ratio as compared to gas-phase oxidation products. Consequently, the overall correlation between O : C ratio and volatility for the full spectrum of SOA products has a low coefficient of determination and wide prediction interval (Table 1, Fig. S1 in the Supplement). Figure S2 in the Supplement shows the summary of O : C ratio vs. volatility, showing that the oxidation products cover almost the full area in this 2-D space. Clear trend has found that volatile compounds have low molar mass, whereas low volatility compounds with low O : C ratio have high molar mass.

Table A1. Experimental conditions in studies identifying oxidation products, as included in Figs. 1 and 4.

	Study	Oxidants	NO	Seed
Dodecane		OH	Low/high	$(NH_4)_2SO_4$
Cyclododecane	This study, Schilling-Fahnestock et al. (2014)	OH	Low/high	$(NH_4)_2SO_4$
Hexylcyclohexane		OH	Low/high	$(NH_4)_2SO_4$
α-pinene	Docherty et al. (2005)	O_3	Low	No seed
	Claeys et al. (2007)	OH	High	No seed
	Claeys et al. (2009)	OH, O_3	High/low	$(NH_4)_2SO_4$, H_2SO_4, $MgSO_4$
	Kahnt et al. (2014)	O_3	High	$(NH_4)_2SO_4$, H_2SO_4
	Kristensen et al. (2014)	OH, O_3	High	$(NH_4)_2SO_4$, H_2SO_4, $MgSO_4$
	Zuend and Seinfeld (2012)	O_3	Low	$(NH_4)_2SO_4$
Limonene	Jaoui et al. (2006)	OH, O_3	High	No seed
	Kundu et al. (2012)	O_3	Low	No seed
Isoprene	Surratt et al. (2006)	OH	High / low	$(NH_4)_2SO_4$, H_2SO_4, no seed
	Surratt et al. (2010)	OH	High / low	$(NH_4)_2SO_4$, H_2SO_4, no seed
	Lin et al (2012)	OH	High	No seed
	Lin et al. (2013)	OH	Low	$(NH_4)_2SO_4$, H_2SO_4, $MgSO_4$

Appendix B: Kinetic regimes for SOA formation

Figure B1 shows a classification scheme for kinetic regimes and limiting cases for SOA formation and aging. Note that the term "limiting case" is reserved for a system that is governed by a single, clearly defined limiting process; the term "kinetic regime" designates a system that is governed by a few (often only one or two) clearly defined rate-limiting processes (Berkemeier et al., 2013). The classification within the particle phase regime (right-hand side of Fig. 3) is explained in detail by Berkemeier et al. (2013). In this study, the gas-phase regime (left-hand side of Fig. 3) extends the classification scheme to SOA formation. The cases of limiting behavior arise from three criteria that are fundamental to formation and partitioning of an oxidation product: (1) the location (gas phase, particle surface, particle bulk) of the reaction leading to SOA formation; (2) the species' saturation ratio (ratio of ambient concentration to saturation concentration) of the oxidation products; and (3) the extent of spatial heterogeneity of the gas and particle phases. Identifying kinetic regimes and limiting cases can be facilitated by an aerosol model, such as the kinetic multi-layer model for gas-particle interactions (KM-GAP) that explicitly resolves mass transport and chemical reactions in the gas and particle phases (Shiraiwa et al., 2012).

B1 Criterion 1: reaction location (gas vs. surface vs. bulk)

Where does formation of oxidation products that contribute to SOA mass predominantly occur, gas phase, particle surface or particle bulk? A two-pronged criterion can be developed. The first sub-criterion evaluates the relative contribution of gas- vs. particle-phase chemistry. The gas- vs. particle-phase contribution ratio (GPCR) can be defined as ratio of the production rate of the oxidation product in the gas phase (P^g) to the total production rate in gas and particle phases ($P^g + P^p$):

$$GPCR = P^g / (P^g + P^p). \tag{B1}$$

As GPCR approaches unity, an oxidation product is produced primarily in the gas phase, and as GPCR approaches zero, it is primarily produced in the particle phase.

If particle-phase chemistry dominates (GPCR ≈ 0), the surface to total particle-phase contribution ratio (STCR) is used to assess the extent to which production occurs predominantly at the surface or in the bulk. STCR can be calculated using the production rate of the oxidation product at the surface (P^s) and in the particle bulk (P^b):

$$STCR = P^s / (P^s + P^b). \tag{B2}$$

If the particle-phase reaction primarily occurs at the surface, STCR approaches unity, and STCR approaches zero if the reaction occurs primarily in the bulk.

B2 Criterion 2: saturation ratio

Is mass transfer of an oxidation product through the gas or into the particle phase limiting SOA growth? After determination of the reaction location, this criterion further classifies the system based on the abundance of oxidation products at the particle surface versus in the near-surface bulk.

In the gas-phase regime, the surface saturation ratio (SSR) can be used to judge the extent to which kinetic limitation of mass transport occurs in the gas phase. With this parameter,
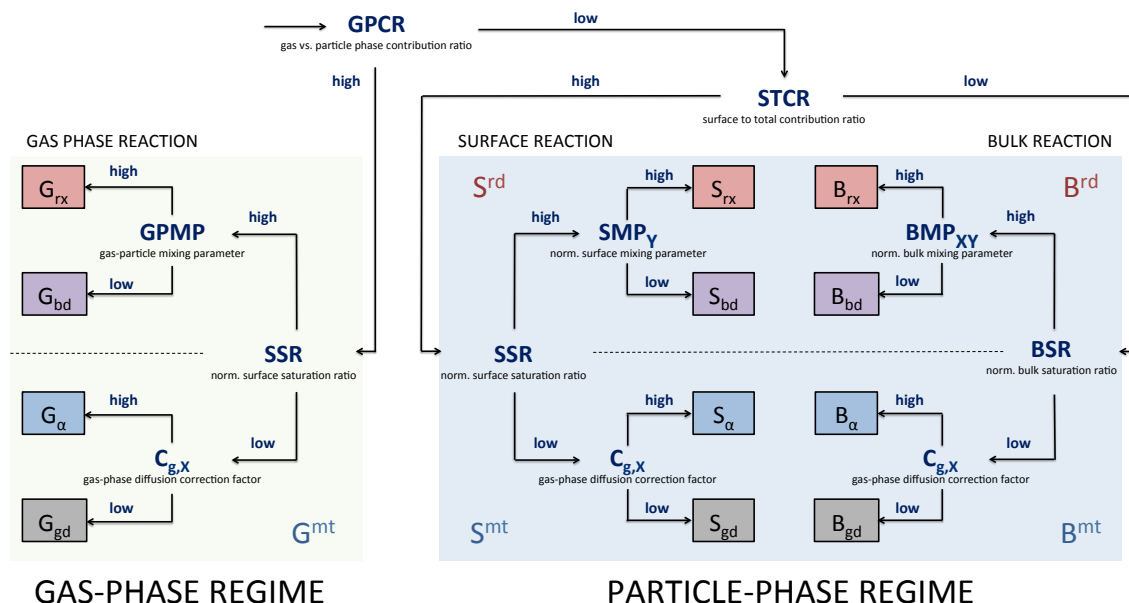
Figure B1. Decision tree for classification and distinction of limiting cases for multiphase chemical evolution of SOA. The classification is based on: (1) the location of the reaction leading to its formation, (2) its saturation ratio, and (3) its mixing parameter to assess the heterogeneity in the gas and particle phases. The resulting limiting cases are shown in the small boxes with reaction location in the gas phase (G), at the surface (S) and in the bulk (B) and limiting processes of chemical reaction (rx), bulk diffusion (bd), mass accommodation (α), and gas-phase diffusion (gd).

the surface concentration of an oxidation product Z, $[Z]_s$, is compared to its surface saturation concentration $[Z]_{s,sat}$. In the absence of reaction or diffusion into the bulk, $[Z]_{s,sat}$ is determined by the gas-phase concentration of Z, $[Z]_g$, and the rates of adsorption and desorption k_a and k_d: $[Z]_{s,sat} = k_a / k_d$ $[Z]_g$ (Pöschl et al., 2007; Berkemeier et al., 2013). The SSR is defined as the ratio of $[Z]_s$ to its saturation concentration at adsorption equilibrium:

$$\text{SSR} = [Z]_s / [Z]_{s,sat}. \tag{B3}$$

The numerical interpretation of SSR is as follows: as SSR approaches zero, the surface is starved of Z, and the system is limited by mass transfer (G^{mt} regime) either by gas-phase diffusion (G_{gd} limiting case) or surface accommodation (G_α limiting case). As SSR approaches unity, the surface is adequately supplied with Z and the system can be limited by production of Z in the gas phase (G_{rx} limiting case) or mass transport into the bulk (G_{bd} limiting case).

In the particle-phase regime, the classification step is based on SSR or the bulk saturation ratio (BSR) to distinguish between systems in the reaction-diffusion regime or the mass-transfer regime (Berkemeier et al., 2013). The BSR is defined analogously to SSR as the ratio of near-surface bulk concentration of an oxidation product to its saturation concentration.

B3   Criterion 3: mixing parameters (MPs)

Is SOA growth limited by diffusion in the gas or particle phase? Depending on the reaction location and saturation ratio, mixing parameters are used to assess the heterogeneity of the gas-particle system. One can define the surface mixing parameter (SMP), the bulk mixing parameter (BMP), the gas-phase diffusion correction factor (C_g), and the gas-particle mixing parameter (GPMP). SMP is defined as the ratio of the actual surface concentration of compound i to the maximum possible surface concentration in the case of perfect particle-phase mixing. BMP is defined using an effective reacto-diffusive length (Berkemeier et al., 2013). As an MP approaches zero, a strong concentration gradient exists and the system is limited by diffusion; as MP approaches unity, the system is well-mixed and limited by reaction.

In mass-transfer limited systems (indicated by a low SR), $C_{g,i}$ distinguishes between gas-phase diffusion limitation and accommodation limitation. $C_{g,i}$ is defined as the ratio of the concentration of compound i in the near-surface gas phase (one mean free path away from the surface) to that in the gas phase far from the particle (Pöschl et al., 2007):

$$C_{g,i} = C_i^{gs} / C_i^g. \tag{B4}$$

As $C_{g,i}$ approaches zero, the compound i exhibits a strong concentration gradient in the gas phase and the system is classified as gas-phase diffusion limited (G_{gd} limiting case); as $C_{g,i}$ approaches unity, the system is designated as accommodation-limited (G_α limiting case).

The gas-particle mixing parameter (GPMP) measures the extent to which the gas-particle system is in quasi-equilibrium and is defined as the ratio of equilibrium gas-phase mass concentration of compound i, $C_i^{g,eq}$, to gas-phase mass concentration, C_i^g (far from particle), which is equivalent to the ratio of particle-phase mass concentration, C_i^{PM}, to equilibrium particle-phase mass concentration, $C_i^{PM,eq}$:

$$\text{GPMP}_i = C_i^{g,eq} / C_i^g = C_i^{PM} / C_i^{PM,eq}. \tag{B5}$$

$C_i^{g,eq}$ and $C_i^{PM,eq}$ can be calculated using an equilibrium partitioning theory (Pankow, 1994; Donahue et al., 2006):

$$C_i^{g,eq} = C_i^* C_i^{PM} / C_{Tot}, \tag{B6}$$

$$C_i^{PM,eq} = C_i^g C_{Tot} / C_i^*, \tag{B7}$$

where C_i^* is the effective saturation mass concentration of compound i, and C_{Tot} is the total particle mass concentration. In the case of ideal mixing, C_i^* is equal to the gas-phase saturation mass concentration over the pure subcooled liquid (C_i^0). Note that $C_i^{g,eq}$ can be regarded as a gas-phase mass concentration just above the particle surface, C_i^s, when Raoult's law is strictly obeyed and C_i^s is in equilibrium with the whole particle (i.e., usually the case for liquid particles).

The value of GPMP determines the extent to which SOA growth is controlled by quasi-equilibrium growth or mass transport limited growth. $C_i^g = C_i^{g,eq}$ (or $C_i^{PM} = C_i^{PM,eq}$) at gas-particle equilibrium. The particle still grows, if C_i^g changes slowly and $C_i^{g,eq}$ follows C_i^g instantaneously (quasi-equilibrium growth) (Shiraiwa and Seinfeld, 2012; Zhang et al., 2012). If $C_i^g > C_i^{g,eq}$, compound i will diffuse from the gas to the particulate phase, driven by concentration or partial pressure gradient between the gas and particle phases (non-equilibrium or mass transport limited growth). Thus, the numerical interpretation of GPMP is: (1) as GPMP approaches 0, SOA growth is limited kinetically by mass transport; (2) as GPMP approaches unity, SOA growth is in quasi-equilibrium and the system is subject to the gas-phase reaction limitation case G_{rx} (the system is limited only by the gas-phase formation rate).

Note that GPMP is small for the limiting cases of G_{bd}, G_α, and G_{gd}. In these limiting cases, SOA growth is still sensitive to the gas-phase formation rate (as it determines the gas-phase concentration), but is limited by interfacial transport, which comprises gas-phase diffusion, surface accommodation, and surface-to-bulk transport processes. Gas-phase diffusion and surface accommodation limitation can be differentiated from surface-to-bulk transport limitation either by SSR or by comparing surface (α_s) and bulk (α_b) accommodation coefficients, each of which is resolved by KM-GAP. α_s is defined as the probability of a molecule sticking to the surface upon collision, whereas α_b is defined as the respective probability of a molecule to enter the bulk of the particle (Pöschl et al., 2007; Shiraiwa et al., 2012). If $\alpha_s \approx \alpha_b$,

then interfacial transport is not limited by surface-to-bulk exchange, and thus is limited by either gas-phase diffusion or surface accommodation; if $\alpha_s > \alpha_b$, then the interfacial transport is limited by surface-to-bulk transport (dissolution or bulk diffusion). For additional discussion of accommodation vs. surface-bulk exchange, see Appendix C in Berkemeier et al. (2013).

## Appendix C: Examples of kinetic regimes and limiting cases

Here we use KM-GAP to model condensation of a semi-volatile compound generated by oxidation of a parent VOC. We assume that the parent VOC with an initial concentration of $10^{10}\,\text{cm}^{-3}$ is converted to a semi-volatile product with a first-order rate coefficient of $0.1\,\text{min}^{-1}$. Conversion of the first-generation product to higher generation products and particle-phase reactions need not be considered. The initial number and mass concentrations of non-volatile pre-existing particles are taken as $10^3\,\text{cm}^{-3}$ and $0.1\,\mu\text{g m}^{-3}$, respectively. The initial particle size distribution is assumed log-normal with a mean diameter of 50 nm and a standard deviation of 1.5. The required kinetic parameters for the simulation are given in Table C1. The gas-phase diffusion coefficient (D_g) of an oxidation product is varied between 0.01–$0.05\,\text{cm}^2\,\text{s}^{-1}$ (Bilde et al., 2003; Bird et al., 2007). The surface accommodation coefficient ($\alpha_{s,0}$) and bulk diffusion coefficient (D_b) are also varied to illustrate the different kinetic regimes and limiting cases for SOA formation in the gas-phase regime.

Figure C1 shows the results of such simulation. The temporal evolution of mass concentration of the parent VOC (black), the oxidation product in the gas phase (C^g, solid blue), in the near-surface gas phase (C^{gs}, dotted blue), in the particle phase (C^{PM}, red), and equilibrium gas-phase concentration ($C^{g,eq}$, dashed blue) are shown. In the simulation presented in Fig. C1a, SOA growth is limited by mass transfer, namely gas-phase diffusion and accommodation (G^{mt} regime, lying between limiting cases G_{gd} and G_α) up to $\sim 10\,\text{s}$, indicated by a low surface saturation ratio (SSR) and a low gas-phase diffusion correction factor ($C_g = C^{gs} / C^g \approx 0.7$). The gas-phase concentration gradient vanishes within $\sim 10\,\text{s}$ ($C^{gs} \approx C^g$), and as C^g continues to increase due to the conversion of the parent VOC, $C^{g,eq}$ follows the change in C^g, essentially instantaneously, and C^{PM} increases. In this case, the gas-phase rate of formation of the oxidation product controls particle growth corresponding to the limiting case of G_{rx} (so-called quasi-equilibrium growth) (Shiraiwa and Seinfeld, 2012; Zhang et al., 2012).

In the simulation presented in Fig. C1b with a relatively low surface accommodation coefficient of 10^{-3}, a steep concentration gradient exhibits between the gas phase and the particle surface ($C^g \approx C^{gs} > C^{g,eq}$) during SOA growth. The system is limited by accommodation (G_α), as SSR is low, but C_g is 1. Figure C1c shows the corresponding results for

Table C1. Properties and kinetic parameters of the VOC oxidation product used in the simulations for SOA growth.

Parameter (unit)	Description	(a)	(b)	(c)	(d)
$\alpha_{s,0}$	Surface accommodation coefficient	1	10^{-3}	1	1
τ_d (s)	Desorption lifetime	10^{-6}	10^{-6}	10^{-6}	10^{-6}
C_0 (μg m^{-3})	Saturation mass concentration	10^3	10^3	10^3	10^{-3}
D_b (cm^2 s^{-1})	Bulk diffusion coefficient	10^{-5}	10^{-5}	10^{-17}	10^{-5}
D_g (cm^2 s^{-1})	Gas-phase diffusion coefficient	0.01	0.05	0.05	0.01
k_g (min^{-1})	First-order gas-phase reaction rate coefficient	0.1	0.1	0.1	0.1
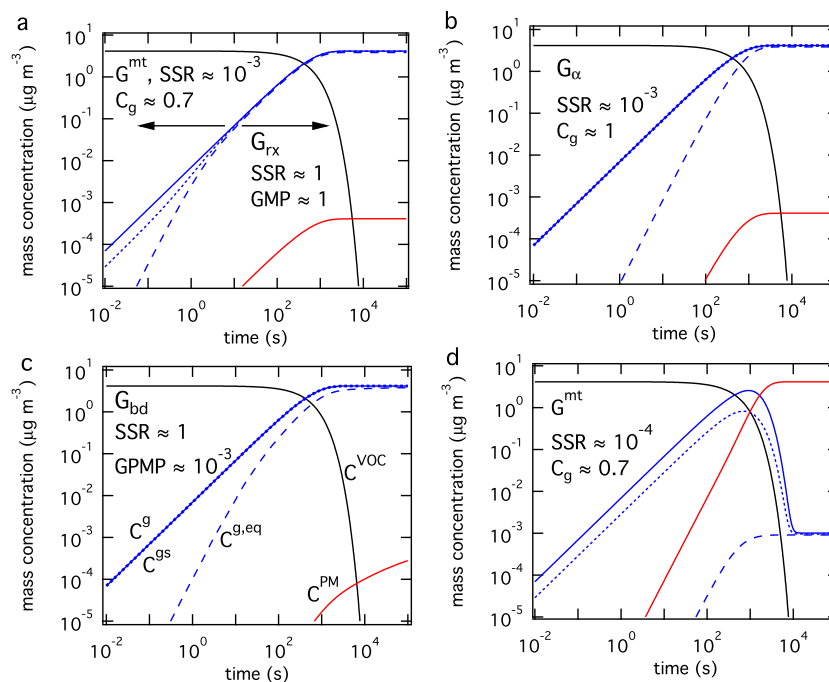
Figure C1. Temporal evolution of mass concentration of the hypothesized VOC oxidation product in the gas phase (solid blue), in the near-surface gas phase (dotted blue), in the particle phase (red), and equilibrium gas-phase concentration (dashed blue). The gas-phase mass concentration of the parent VOC is shown by the black line. For semi-volatile oxidation products with $C^* = 10^3\,\mu$g m^{-3}, SOA growth is limited by **(a)** gas-phase reaction (G$_{rx}$), **(b)** accommodation (G$_\alpha$), and **(c)** bulk diffusion (G$_{bd}$). **(d)** shows an exemplary simulation for LVOCs, with $C^* = 10^{-3}\,\mu$g m^{-3} exhibiting kinetic limitation in the gas-particle mass transfer regime (G^{mt}).

particles in an amorphous, semi-solid state with the low bulk diffusion coefficient of 10^{-17} cm^2 s^{-1}. In this case, particle growth is limited by surface-to-bulk transport (G$_{bd}$), as SSR is high and GPMP is low. Note that GPMP refers to the gap between C^g and $C^{g,eq}$. The bulk accommodation coefficient α_b is $\sim 10^{-5}$, which is much smaller than the surface accommodation coefficient α_s. Sensitivity studies with varying D_b reveal that, when $D_b < \sim 10^{-15}$ cm^2 s^{-1}, the time scales for surface-bulk exchange and bulk diffusion become longer than that of gas-phase diffusion and accommodation (Shiraiwa and Seinfeld, 2012). From the Stokes–Einstein relation, this value corresponds to a viscosity of $\sim 10^7$ Pa s, which is on the same order as the viscosity of α-pinene SOA at 40 % RH (relative humidity) (Renbaum-Wolff et al., 2013). Thus, SOA growth can be limited by bulk diffusion at low

RH, whereas surface accommodation becomes more important at high RH.

Figure C1d shows the simulation for gas-phase formation and partitioning of low volatility oxidation products ($C_0 = 10^{-3}\,\mu$g m^{-3}) into liquid particles. SSR is low over the course of particle growth, indicating persistence of a strong concentration gradient between the gas phase and the particle surface. The gas-phase diffusion correction factor (C_g) stays at 0.7 up to $\sim 10^3$ s, indicating that near-surface gas phase concentration [Z]$_{gs}$ is depleted by 30 % compared to gas phase concentration [Z]$_g$ due to rapid uptake and slow gas diffusion ($D_g = 0.01$ cm^2 s^{-1}). C_g decreases substantially down to ~ 0.2 only when gas-phase formation ceases at $\sim 10^3$–10^4 s. Overall, SOA growth is limited by mass transfer (gas-phase diffusion and accommodation;

G^{mt} regime). When a very low-bulk diffusivity is assumed ($D_b \approx 10^{-19}$ cm^2 s^{-1}; figure not shown), SSR is close to 1 and GPMP is very low during particle growth. Thus, the system is limited by bulk diffusion (G$_{bd}$). Consequently, partitioning of low volatility compounds could be limited by bulk diffusion, when organic particles adopt amorphous solid state (Shiraiwa and Seinfeld, 2012; Zaveri et al., 2014).

Appendix D: Application to chamber data – dodecane photooxidation

Here we apply the classification scheme to experimental data on SOA formation from oxidation of the C_{12} alkane, dodecane ($C_{12}H_{28}$) in the Caltech environmental chamber (Yee et al., 2012). 34 ppb dodecane was oxidized by OH radicals over 20 h in the presence of dry ammonium sulfate seed particles at low concentrations of NO$_x$, typical of non-urban conditions. KM-GAP was used to simulate the evolution of SOA mass, the organic atomic oxygen-to-carbon (O : C) ratio, and particle-size distribution in the chamber experiments (Shiraiwa et al., 2013a). In the gas phase, SVOCs resulting from up to five generations of OH oxidation are considered. Some of the fourth generation products have been established to be multifunctional carbonyl compounds (aldehydes) that can react in the particle phase with hydroperoxide, hydroxyl, and peroxycarboxylic acid groups, forming peroxyhemiacetal (PHA), hemiacetal, and acylperoxyhemiacetal, respectively (Docherty et al., 2005; Yee et al., 2012; Ziemann and Atkinson, 2012). The observed evolution of the particle size distribution is simulated successfully only if such particle-phase chemistry is included (Shiraiwa et al., 2013a).

Figure 5 shows the span of molar mass and gas-phase saturation concentrations over the pure subcooled liquids (C_i^0) for gas-phase oxidation products and particle-phase products of the dodecane system. The smaller symbols indicate individual products predicted in the dodecane photooxidation chemical mechanism (Yee et al., 2012) and the large solid circles indicate the surrogate compounds used in the KM-GAP simulations (Shiraiwa et al., 2013a). Upon gas-phase multi-generation oxidation, the volatility of SVOCs decreases from $\sim 10^6 \mu$g m^{-3} (dodecane) to $\sim 1 \mu$g m^{-3}. The particle-phase products have significantly lower volatilities of $\sim 10^{-2} \mu$g m^{-3}.

Figure D1a and b show the temporal evolution of mass concentration of the first and fifth generation oxidation products in the gas phase (C^g), at the particle surface (C^s), and in the particle phase (C^{PM}). C^g is slightly higher than $C^{g,eq}$ up to ~ 5 h due to continuous generation of oxidation products in the gas phase, and eventually reaching $C^g \approx C^{g,eq}$ for both products (GPMP ≈ 1). Note that mass concentration in the near-surface gas phase (C^{gs}) is identical to C^g, indicating that gas-phase diffusion is not a limiting step. The same trend is seen for other generation products. Thus, the contribution of gas-phase semi-volatile oxidation products to SOA formation is limited by their formation in the gas phase, corresponding to the limiting case of G$_{rx}$.

Particle-phase products are formed by the reaction of reactive aldehydes with SVOCs in the particle phase. Simulations suggest that this reaction occurs mainly at the surface and in the near-surface bulk (Shiraiwa et al., 2013a). Aldehydes and SVOCs are both saturated in the bulk (BSR is high). A strong concentration gradient of aldehydes in the bulk is predicted, whereas SVOCs are predicted to be essentially homogeneous in the bulk (BMP$_{XY} \approx 0.5$). Bulk reaction is tightly coupled with bulk diffusion, and the system falls into the reaction-diffusion regime (SBrd), particularly the traditional reacto-diffusive case (B$^{rd}_{trad}$) (Worsnop et al., 2002; Pöschl et al., 2007; Kolb et al., 2010; Berkemeier et al., 2013).
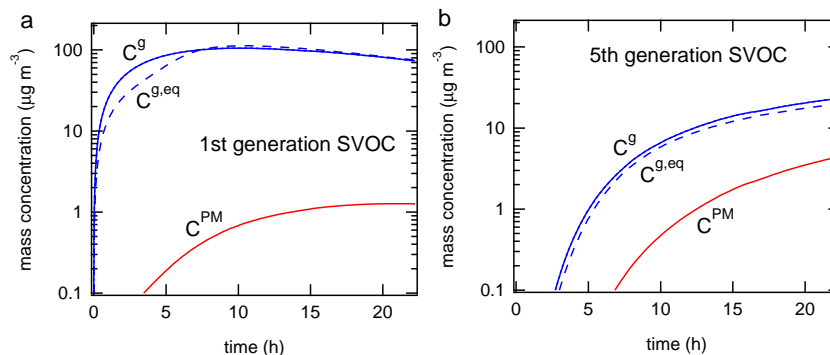
Figure D1. Modeling SOA formation from dodecane photooxidation. Temporal evolution of mass concentration of the **(a)** first and **(b)** five generation products in the gas phases (solid blue), particle phases (red), and equilibrium gas-phase mass concentration (dashed blue).
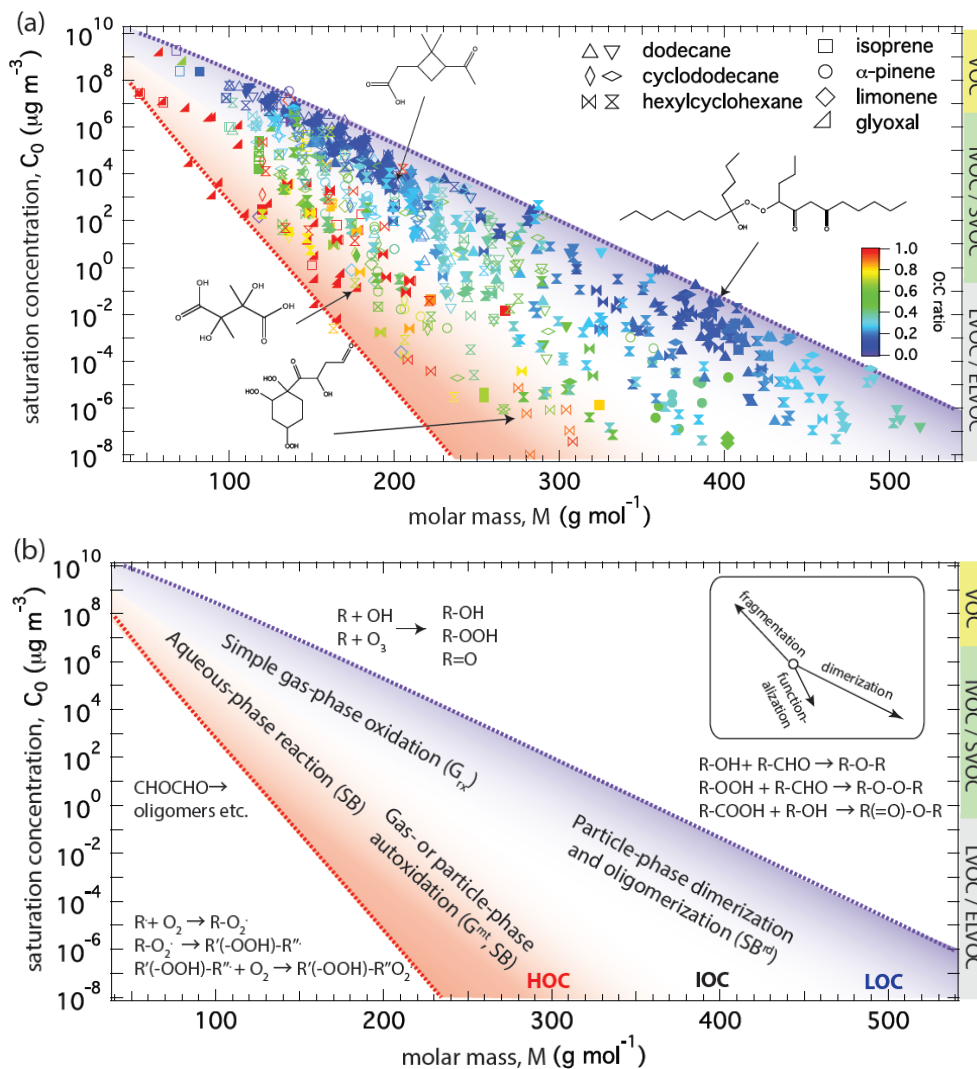
Figure D2. Alternative representation of molecular corridors (Fig. 4) displaying volatility (C_0) as a function of molar mass, which appears more straightforward to use and interpret in mechanistic studies (see Fig. 5) and for direct comparison to mass spectra. Volatility decreases as molar mass increases from left to right, and the slope $d\log C_0 / dM$ is steeper for molecules with higher O : C ratio and polarity due to stronger hydrogen bonding and evaporation enthalpy.

References

Abramson, E., Imre, D., Beranek, J., Wilson, J. M., and Zelenyuk,
A.: Experimental determination of chemical diffusion within sec-
ondary organic aerosol particles, Phys. Chem. Chem. Phys., 15,
2983–2991, 2013.

Berkemeier, T., Huisman, A. J., Ammann, M., Shiraiwa, M., Koop,
T., and Pöschl, U.: Kinetic regimes and limiting cases of gas
uptake and heterogeneous reactions in atmospheric aerosols and
clouds: a general classification scheme, Atmos. Chem. Phys., 13,
6663–6686, doi:10.5194/acp-13-6663-2013, 2013.

Bertram, A. K., Ivanov, A. V., Hunter, M., Molina, L. T., and
Molina, M. J.: The reaction probability of OH on organic sur-
faces of tropospheric interest, J. Phys. Chem. A, 105, 9415–9421,
2001.

Bilde, M., Svenningsson, B., Monster, J., and Rosenorn, T.: Even-
odd alternation of evaporation rates and vapor pressures of C3-
C9 dicarboxylic acid aerosols, Environ. Sci. Technol., 37, 1371–
1378, 2003.

Bird, R. B., Stewart, W. E., and Lightfoot, E. N.: Transport Phe-
nomena, 2nd edition, John Wiley & Sons, Inc., New York, 2007.

Cappa, C. D. and Wilson, K. R.: Evolution of organic aerosol mass
spectra upon heating: implications for OA phase and partitioning
behavior, Atmos. Chem. Phys., 11, 1895–1911, doi:10.5194/acp-
11-1895-2011, 2011.

Carlton, A. G., Turpin, B. J., Altieri, K. E., Seitzinger, S., Reff, A.,
Lim, H. J., and Ervens, B.: Atmospheric oxalic acid and SOA
production from glyoxal: Results of aqueous photooxidation ex-
periments, Atmos. Environ., 41, 7588–7602, 2007.

Chan, M. N., Nah, T., and Wilson, K. R.: Real time in situ chemi-
cal characterization of sub-micron organic aerosols using Direct
Analysis in Real Time mass spectrometry (DART-MS): the effect
of aerosol size and volatility, Analyst, 138, 3749–3757, 2013.

Chang, E. I. and Pankow, J. F.: Prediction of activity coefficients in
liquid aerosol particles containing organic compounds, dissolved
inorganic salts, and water – Part 2: Consideration of phase sep-
aration effects by an X-UNIFAC model, Atmos. Environ., 40,
6422–6436, 2006.

Claeys, M., Szmigielski, R., Kourtchev, I., Van der Veken, P.,
Vermeylen, R., Maenhaut, W., Jaoui, M., Kleindienst, T. E.,

Lewandowski, M., Offenberg, J. H., and Edney, E. O.: Hydroxy-
dicarboxylic acids: Markers for secondary organic aerosol from
the photooxidation of alpha-pinene, Environ. Sci. Technol., 41,
1628–1634, 2007.

Claeys, M., Iinuma, Y., Szmigielski, R., Surratt, J. D., Blockhuys,
F., Van Alsenoy, C., Boege, O., Sierau, B., Gomez-Gonzalez, Y.,
Vermeylen, R., Van der Veken, P., Shahgholi, M., Chan, A. W.
H., Herrmann, H., Seinfeld, J. H., and Maenhaut, W.: Terpenylic
Acid and Related Compounds from the Oxidation of alpha-
Pinene: Implications for New Particle Formation and Growth
above Forests, Environ. Sci. Technol., 43, 6976–6982, 2009.

Compernolle, S., Ceulemans, K., and Muller, J. F.: EVAPORA-
TION: a new vapour pressure estimation methodfor organic
molecules including non-additivity and intramolecular interac-
tions, Atmos. Chem. Phys., 11, 9431–9450, doi:10.5194/acp-11-
9431-2011, 2011.

Crounse, J. D., Nielsen, L. B., Jørgensen, S., Kjaergaard, H. G.,
and Wennberg, P. O.: Autoxidation of organic compounds in the
atmosphere, J. Phys. Chem. Lett., 4, 3513–3520, 2013.

Docherty, K. S., Wu, W., Lim, Y. B., and Ziemann, P. J.: Contri-
butions of organic peroxides to secondary aerosol formed from
reactions of monoterpenes with O$_3$, Environ. Sci. Technol., 39,
4049–4059, 2005.

Donahue, N. M., Robinson, A. L., Stanier, C. O., and Pandis,
S. N.: Coupled partitioning, dilution, and chemical aging of
semivolatile organics, Environ. Sci. Technol., 40, 2635–2643,
2006.

Donahue, N. M., Epstein, S. A., Pandis, S. N., and Robinson, A.
L.: A two-dimensional volatility basis set: 1. organic–aerosol
mixing thermodynamics, Atmos. Chem. Phys., 11, 3303–3318,
doi:10.5194/acp-11-3303-2011, 2011.

Donahue, N. M., Henry, K. M., Mentel, T. F., Kiendler-Scharr, A.,
Spindler, C., Bohn, B., Brauers, T., Dorn, H. P., Fuchs, H., Till-
mann, R., Wahner, A., Saathoff, H., Naumann, K.-H., Möhler,
O., Leisner, T., Müller, L., Reinnig, M.-C., Hoffmann, T., Salo,
K., Hallquist, M., Frosch, M., Bilde, M., Tritscher, T., Barmet, P.,
Praplan, A. P., DeCarlo, P. F., Dommen, J., Prévôt, A. S. H., and
Baltensperger, U.: Aging of biogenic secondary organic aerosol
via gas-phase OH radical reactions, P. Natl. Acad. Sci. USA, 109,
13503–13508, 2012.

Ehn, M., Kleist, E., Junninen, H., Petaja, T., Lonn, G., Schobes-
berger, S., Dal Maso, M., Trimborn, A., Kulmala, M., Worsnop,
D. R., Wahner, A., Wildt, J., and Mentel, T. F.: Gas phase
formation of extremely oxidized pinene reaction products in
chamber and ambient air, Atmos. Chem. Phys., 12, 5113–5127,
doi:10.5194/acp-12-5113-2012, 2012.

Ehn, M., Thornton, J. A., Kleist, E., Sipila, M., Junninen, H., Pulli-
nen, I., Springer, M., Rubach, F., Tillmann, R., Lee, B., Lopez-
Hilfiker, F., Andres, S., Acir, I.-H., Rissanen, M., Jokinen, T.,
Schobesberger, S., Kangasluoma, J., Kontkanen, J., Nieminen,
T., Kurten, T., Nielsen, L. B., Jorgensen, S., Kjaergaard, H. G.,
Canagaratna, M., Dal Maso, M., Berndt, T., Petaja, T., Wahner,
A., Kerminen, V.-M., Kulmala, M., Worsnop, D. R., Wildt, J.,
and Mentel, T. F.: A large source of low-volatility secondary or-
ganic aerosol, Nature, 506, 476–479, 2014.

Ervens, B. and Volkamer, R.: Glyoxal processing by aerosol multi-
phase chemistry: towards a kinetic modeling framework of sec-
ondary organic aerosol formation in aqueous particles, Atmos.

Chem. Phys., 10, 8219–8244, doi:10.5194/acp-10-8219-2010, 2010.

Ervens, B., Turpin, B. J., and Weber, R. J.: Secondary organic aerosol formation in cloud droplets and aqueous particles (aqSOA): a review of laboratory, field and model studies, Atmos. Chem. Phys., 11, 11069–11102, doi:10.5194/acp-11-11069-2011, 2011.

Goldstein, A. H. and Galbally, I. E.: Known and unexplored organic constituents in the earth's atmosphere, Environ. Sci. Technol., 41, 1514–1521, 2007.

Hallquist, M., Wenger, J. C., Baltensperger, U., Rudich, Y., Simpson, D., Claeys, M., Dommen, J., Donahue, N. M., George, C., Goldstein, A. H., Hamilton, J. F., Herrmann, H., Hoffmann, T., Iinuma, Y., Jang, M., Jenkin, M. E., Jimenez, J. L., Kiendler-Scharr, A., Maenhaut, W., McFiggans, G., Mentel, T. F., Monod, A., Prevot, A. S. H., Seinfeld, J. H., Surratt, J. D., Szmigielski, R., and Wildt, J.: The formation, properties and impact of secondary organic aerosol: current and emerging issues, Atmos. Chem. Phys., 9, 5155–5235, doi:10.5194/acp-9-5155-2009, 2009.

Hosny, N. A., Fitzgerald, C., Tong, C., Kalberer, M., Kuimova, M. K., and Pope, F. D.: Fluorescent lifetime imaging of atmospheric aerosols: a direct probe of aerosol viscosity, Faraday Discuss., 165, 343–356, 2013.

Iinuma, Y., Boge, O., Gnauk, T., and Herrmann, H.: Aerosol-chamber study of the alpha-pinene/O_3 reaction: influence of particle acidity on aerosol yields and products, Atmos. Environ., 38, 761–773, 2004.

Iinuma, Y., Muller, C., Berndt, T., Boge, O., Claeys, M., and Herrmann, H.: Evidence for the existence of organosulfates from beta-pinene ozonolysis in ambient secondary organic aerosol, Environ. Sci. Technol., 41, 6678-6683, 2007.

Jang, M. S., Czoschke, N. M., Lee, S., and Kamens, R. M.: Heterogeneous atmospheric aerosol production by acid-catalyzed particle-phase reactions, Science, 298, 814–817, 2002.

Jaoui, M., Corse, E., Kleindienst, T. E., Offenberg, J. H., Lewandowski, M., and Edney, E. O.: Analysis of secondary organic aerosol compounds from the photooxidation of d-limonene in the presence of NO_x and their detection in ambient PM2.5, Environ. Sci. Technol., 40, 3819–3828, 2006.

Jimenez, J. L., Canagaratna, M. R., Donahue, N. M., Prevot, A. S. H., Zhang, Q., Kroll, J. H., DeCarlo, P. F., Allan, J. D., Coe, H., Ng, N. L., Aiken, A. C., Docherty, K. S., Ulbrich, I. M., Grieshop, A. P., Robinson, A. L., Duplissy, J., Smith, J. D., Wilson, K. R., Lanz, V. A., Hueglin, C., Sun, Y. L., Tian, J., Laaksonen, A., Raatikainen, T., Rautiainen, J., Vaattovaara, P., Ehn, M., Kulmala, M., Tomlinson, J. M., Collins, D. R., Cubison, M. J., Dunlea, E. J., Huffman, J. A., Onasch, T. B., Alfarra, M. R., Williams, P. I., Bower, K., Kondo, Y., Schneider, J., Drewnick, F., Borrmann, S., Weimer, S., Demerjian, K., Salcedo, D., Cottrell, L., Griffin, R., Takami, A., Miyoshi, T., Hatakeyama, S., Shimono, A., Sun, J. Y., Zhang, Y. M., Dzepina, K., Kimmel, J. R., Sueper, D., Jayne, J. T., Herndon, S. C., Trimborn, A. M., Williams, L. R., Wood, E. C., Middlebrook, A. M., Kolb, C. E., Baltensperger, U., and Worsnop, D. R.: Evolution of organic aerosols in the atmosphere, Science, 326, 1525–1529, 2009.

Kahnt, A., Iinuma, Y., Blockhuys, F., Mutzel, A., Vermeylen, R., Kleindienst, T. E., Jaoui, M., Offenberg, J. H., Lewandowski, M., Böge, O., Herrmann, H., Maenhaut, W., and Claeys, M.: 2-Hydroxyterpenylic acid: An oxygenated marker compound for

α-pinene secondary organic aerosol in ambient fine aerosol, Environ. Sci. Technol., 48, 4901–4908, 2014.

Kalberer, M., Sax, M., and Samburova, V.: Molecular size evolution of oligomers in organic aerosols collected in urban atmospheres and generated in a smog chamber, Environ. Sci. Technol., 40, 5917–5922, 2006.

Kampf, C. J., Waxman, E. M., Slowik, J. G., Dommen, J., Pfaffenberger, L., Praplan, A. P., Prevot, A. S. H., Baltensperger, U., Hoffmann, T., and Volkamer, R.: Effective Henry's Law Partitioning and the Salting Constant of Glyoxal in Aerosols Containing Sulfate, Environ. Sci. Technol., 47, 4236–4244, 2013.

Kolb, C. E., Cox, R. A., Abbatt, J. P. D., Ammann, M., Davis, E. J., Donaldson, D. J., Garrett, B. C., George, C., Griffiths, P. T., Hanson, D. R., Kulmala, M., McFiggans, G., Pöschl, U., Riipinen, I., Rossi, M. J., Rudich, Y., Wagner, P. E., Winkler, P. M., Worsnop, D. R., and O' Dowd, C. D.: An overview of current issues in the uptake of atmospheric trace gases by aerosols and clouds, Atmos. Chem. Phys., 10, 10561–10605, doi:10.5194/acp-10-10561-2010, 2010.

Koop, T., Bookhold, J., Shiraiwa, M., and Pöschl, U.: Glass transition and phase state of organic compounds: dependency on molecular properties and implications for secondary organic aerosols in the atmosphere, Phys. Chem. Chem. Phys., 13, 19238–19255, 2011.

Kristensen, K., Cui, T., Zhang, H., Gold, A., Glasius, M., and Surratt, J. D.: Dimer esters in α-pinene secondary organic aerosol: effect of hydroxyl radical, ozone, relative humidity and aerosol acidity, Atmos. Chem. Phys., 14, 4201–4218, doi:10.5194/acp-14-4201-2014, 2014.

Kroll, J. H. and Seinfeld, J. H.: Chemistry of secondary organic aerosol: Formation and evolution of low-volatility organics in the atmosphere, Atmos. Environ., 42, 3593–3624, 2008.

Kundu, S., Fisseha, R., Putman, A. L., Rahn, T. A., and Mazzoleni, L. R.: High molecular weight SOA formation during limonene ozonolysis: insights from ultrahigh-resolution FT-ICR mass spectrometry characterization, Atmos. Chem. Phys., 12, 5523–5536, doi:10.5194/acp-12-5523-2012, 2012.

Kuwata, M. and Martin, S. T.: Phase of atmospheric secondary organic material affects its reactivity, P. Natl. Acad. Sci. USA, 109, 17354–17359, 2012.

Laskin, A., Laskin, J., and Nizkorodov, S. A.: Mass spectrometric approaches for chemical characterisation of atmospheric aerosols: critical review of the most recent advances, Environ. Chem., 9, 163–189, 2012a.

Laskin, J., Eckert, P. A., Roach, P. J., Heath, B. S., Nizkorodov, S. A., and Laskin, A.: Chemical Analysis of Complex Organic Mixtures Using Reactive Nanospray Desorption Electrospray Ionization Mass Spectrometry, Anal. Chem., 84, 7179–7187, 2012b.

Liggio, J., Li, S. M., and McLaren, R.: Heterogeneous reactions of glyoxal on particulate matter: Identification of acetals and sulfate esters, Environ. Sci. Technol., 39, 1532–1541, 2005.

Lim, Y. B., Tan, Y., Perri, M. J., Seitzinger, S. P., and Turpin, B. J.: Aqueous chemistry and its role in secondary organic aerosol (SOA) formation, Atmos. Chem. Phys., 10, 10521–10539, doi:10.5194/acp-10-10521-2010, 2010.

Lin, Y.-H., Zhang, Z., Docherty, K. S., Zhang, H., Budisulistiorini, S. H., Rubitschun, C. L., Shaw, S. L., Knipping, E. M., Edgerton, E. S., Kleindienst, T. E., Gold, A., and Surratt, J. D.: Isoprene Epoxydiols as Precursors to Secondary Organic Aerosol

Formation: Acid-Catalyzed Reactive Uptake Studies with Authentic Compounds, Environ. Sci. Technol., 46, 250-258, 2012.

Lin, Y.-H., Zhang, H., Pye, H. O. T., Zhang, Z., Marth, W. J., Park, S., Arashiro, M., Cui, T., Budisulistiorini, S. H., Sexton, K. G., Vizuete, W., Xie, Y., Luecken, D. J., Piletic, I. R., Edney, E. O., Bartolotti, L. J., Gold, A., and Surratt, J. D.: Epoxide as a precursor to secondary organic aerosol formation from isoprene photooxidation in the presence of nitrogen oxides, P. Natl. Acad. Sci. USA, 110, 6718–6723, 2013.

Loza, C. L., Craven, J. S., Yee, L. D., Coggon, M. M., Schwantes, R. H., Shiraiwa, M., Zhang, X., Schilling, K. A., Ng, N. L., Canagaratna, M. R., Ziemann, P. J., Flagan, R. C., and Seinfeld, J. H.: Secondary organic aerosol yields of 12-carbon alkanes, Atmos. Chem. Phys., 14, 1423–1439, doi:10.5194/acp-14-1423-2014, 2014.

McNeill, V. F., Woo, J. L., Kim, D. D., Schwier, A. N., Wannell, N. J., Sumner, A. J., and Barakat, J. M.: Aqueous-phase secondary organic aerosol and organosulfate formation in atmospheric aerosols: A modeling study, Environ. Sci. Technol., 46, 8075–8081, 2012.

Murphy, B. N., Donahue, N. M., Robinson, A. L., and Pandis, S. N.: A naming convention for atmospheric organic aerosol, Atmos. Chem. Phys., 14, 5825–5839, doi:10.5194/acp-14-5825-2014, 2014.

Nguyen, T. B., Laskin, J., Laskin, A., and Nizkorodov, S. A.: Nitrogen-Containing Organic Compounds and Oligomers in Secondary Organic Aerosol Formed by Photooxidation of Isoprene, Environ. Sci. Technol., 45, 6908–6918, 2011.

Nguyen, T. B., Nizkorodov, S. A., Laskin, A., and Laskin, J.: An approach toward quantification of organic compounds in complex environmental samples using high-resolution electrospray ionization mass spectrometry, Anal. Methods, 5, 72–80, 2013.

Offenberg, J. H., Lewandowski, M., Edney, E. O., Kleindienst, T. E., and Jaoui, M.: Influence of Aerosol Acidity on the Formation of Secondary Organic Aerosol from Biogenic Precursor Hydrocarbons, Environ. Sci. Technol., 43, 7742–7747, 2009.

Pankow, J. F.: An absorption-model of the gas aerosol partitioning involved in the formation of secondary organic aerosol, Atmos. Environ., 28, 189–193, 1994.

Perraud, V., Bruns, E. A., Ezell, M. J., Johnson, S. N., Yu, Y., Alexander, M. L., Zelenyuk, A., Imre, D., Chang, W. L., Dabdub, D., Pankow, J. F., and Finlayson-Pitts, B. J.: Nonequilibrium atmospheric secondary organic aerosol formation and growth, P. Natl. Acad. Sci. USA, 109, 2836–2841, 2012.

Pfrang, C., Shiraiwa, M., and Pöschl, U.: Chemical ageing and transformation of diffusivity in semi-solid multi-component organic aerosol particles, Atmos. Chem. Phys., 11, 7343–7354, doi:10.5194/acp-11-7343-2011, 2011.

Pierce, J. R., Riipinen, I., Kulmala, M., Ehn, M., Petäjä, T., Junninen, H., Worsnop, D. R., and Donahue, N. M.: Quantification of the volatility of secondary organic compounds in ultrafine particles during nucleation events, Atmos. Chem. Phys., 11, 9019–9036, doi:10.5194/acp-11-9019-2011, 2011.

Pöschl, U., Rudich, Y., and Ammann, M.: Kinetic model framework for aerosol and cloud surface chemistry and gas-particle interactions – Part 1: General equations, parameters, and terminology, Atmos. Chem. Phys., 7, 5989–6023, doi:10.5194/acp-7-5989-2007, 2007.

Presto, A. A., Hartz, K. E. H., and Donahue, N. M.: Secondary organic aerosol production from terpene ozonolysis. 2. Effect of NO$_X$ concentration, Environ. Sci. Technol., 39, 7046–7054, 2005.

Renbaum-Wolff, L., Grayson, J. W., Bateman, A. P., Kuwata, K., Sellier, M., Murray, B. J., Schilling, J. E., Martin, S. T., and Bertram, A. K.: Viscosity of α-pinene secondary organic material and implications for particle growth and reactivity, P. Natl. Acad. Sci. USA, 110, 8014–8019, 2013.

Riipinen, I., Pierce, J. R., Yli-Juuti, T., Nieminen, T., Hakkinen, S., Ehn, M., Junninen, H., Lehtipalo, K., Petaja, T., Slowik, J., Chang, R., Shantz, N. C., Abbatt, J., Leaitch, W. R., Kerminen, V. M., Worsnop, D. R., Pandis, S. N., Donahue, N. M., and Kulmala, M.: Organic condensation: a vital link connecting aerosol formation to cloud condensation nuclei (CCN) concentrations, Atmos. Chem. Phys., 11, 3865–3878, doi:10.5194/acp-11-3865-2011, 2011.

Sareen, N., Schwier, A. N., Shapiro, E. L., Mitroo, D., and McNeill, V. F.: Secondary organic material formed by methylglyoxal in aqueous aerosol mimics, Atmos. Chem. Phys., 10, 997–1016, doi:10.5194/acp-10-997-2010, 2010.

Schilling-Fahnestock, K. A., Yee, L. D., Loza, C. L., Coggon, M. M., Schwantes, R., Zhang, X., Dalleska, N. F., and Seinfeld, J. H.: Secondary Organic Aerosol Composition from C_{12} Alkanes, J. Phys. Chem. A, doi:10.1021/jp501779w, 2014.

Schobesberger, S., Junninen, H., Bianchi, F., Lonn, G., Ehn, M., Lehtipalo, K., Dommen, J., Ehrhart, S., Ortega, I. K., Franchin, A., Nieminen, T., Riccobono, F., Hutterli, M., Duplissy, J., Almeida, J., Amorim, A., Breitenlechner, M., Downard, A. J., Dunne, E. M., Flagan, R. C., Kajos, M., Keskinen, H., Kirkby, J., Kupc, A., Kuerten, A., Kurten, T., Laaksonen, A., Mathot, S., Onnela, A., Praplan, A. P., Rondo, L., Santos, F. D., Schallhart, S., Schnitzhofer, R., Sipila, M., Tome, A., Tsagkogeorgas, G., Vehkamaki, H., Wimmer, D., Baltensperger, U., Carslaw, K. S., Curtius, J., Hansel, A., Petaja, T., Kulmala, M., Donahue, N. M., and Worsnop, D. R.: Molecular understanding of atmospheric particle formation from sulfuric acid and large oxidized organic molecules, P. Natl. Acad. Sci. USA, 110, 17223–17228, 2013.

Shiraiwa, M., Ammann, M., Koop, T., and Pöschl, U.: Gas uptake and chemical aging of semisolid organic aerosol particles, P. Natl. Acad. Sci. USA, 108, 11003–11008, 2011.

Shiraiwa, M., Pfrang, C., Koop, T., and Pöschl, U.: Kinetic multi-layer model of gas-particle interactions in aerosols and clouds (KM-GAP): linking condensation, evaporation and chemical reactions of organics, oxidants and water, Atmos. Chem. Phys., 12, 2777–2794, doi:10.5194/acp-12-2777-2012, 2012.

Shiraiwa, M. and Seinfeld, J. H.: Equilibration timescale of atmospheric secondary organic aerosol partitioning, Geophys. Res. Lett., 39, L24801, doi:10.1029/2012GL054008, 2012.

Shiraiwa, M., Yee, L. D., Schilling, K. A., Loza, C. L., Craven, J. S., Zuend, A., Ziemann, P. J., and Seinfeld, J. H.: Size distribution dynamics reveal particle-phase chemistry in organic aerosol formation, P. Natl. Acad. Sci. USA, 110, 11746–11750, 2013a.

Shiraiwa, M., Zuend, A., Bertram, A. K., and Seinfeld, J. H.: Gas-particle partitioning of atmospheric aerosols: interplay of physical state, non-ideal mixing and morphology, Phys. Chem. Chem. Phys., 15, 11441–11453, 2013b.

Surratt, J. D., Murphy, S. M., Kroll, J. H., Ng, N. L., Hildebrandt, L., Sorooshian, A., Szmigielski, R., Vermeylen, R., Maenhaut,

W., Claeys, M., Flagan, R. C., and Seinfeld, J. H.: Chemical composition of secondary organic aerosol formed from the photooxidation of isoprene, J. Phys. Chem. A, 110, 9665–9690, 2006.

Surratt, J. D., Gomez-Gonzalez, Y., Chan, A. W. H., Vermeylen, R., Shahgholi, M., Kleindienst, T. E., Edney, E. O., Offenberg, J. H., Lewandowski, M., Jaoui, M., Maenhaut, W., Claeys, M., Flagan, R. C., and Seinfeld, J. H.: Organosulfate formation in biogenic secondary organic aerosol, J. Phys. Chem. A, 112, 8345–8378, 2008.

Surratt, J. D., Chan, A. W. H., Eddingsaas, N. C., Chan, M. N., Loza, C. L., Kwan, A. J., Hersey, S. P., Flagan, R. C., Wennberg, P. O., and Seinfeld, J. H.: Reactive intermediates revealed in secondary organic aerosol formation from isoprene, P. Natl. Acad. Sci. USA, 107, 6640–6645, 2010.

Trump, E. R. and Donahue, N. M.: Oligomer formation within secondary organic aerosols: equilibrium and dynamic considerations, Atmos. Chem. Phys., 14, 3691–3701, doi:10.5194/acp-14-3691-2014, 2014.

Vaden, T. D., Imre, D., Beranek, J., Shrivastava, M., and Zelenyuk, A.: Evaporation kinetics and phase of laboratory and ambient secondary organic aerosol, P. Natl. Acad. Sci. USA, 108, 2190–2195, 2011.

Virtanen, A., Joutsensaari, J., Koop, T., Kannosto, J., YliPirilä, P., Leskinen, J., Mäkelä, J. M., Holopainen, J. K., Pöschl, U., Kulmala, M., Worsnop, D. R., and Laaksonen, A.: An amorphous solid state of biogenic secondary organic aerosol particles, Nature, 467, 824–827, 2010.

Vogel, A. L., Äijälä, M., Corrigan, A. L., Junninen, H., Ehn, M., Petäjä, T., Worsnop, D. R., Kulmala, M., Russell, L. M., Williams, J., and Hoffmann, T.: In situ submicron organic aerosol characterization at a boreal forest research station during HUMPPA-COPEC 2010 using soft and hard ionization mass spectrometry, Atmos. Chem. Phys., 13, 10933–10950, doi:10.5194/acp-13-10933-2013, 2013.

Williams, B. J., Goldstein, A. H., Kreisberg, N. M., and Hering, S. V.: In situ measurements of gas/particle-phase transitions for atmospheric semivolatile organic compounds, P. Natl. Acad. Sci. USA, 107, 6676–6681, 2010.

Worsnop, D. R., Morris, J. W., Shi, Q., Davidovits, P., and Kolb, C. E.: A chemical kinetic model for reactive transformations of aerosol particles, Geophys. Res. Lett., 29, 1–4, 2002.

Xu, L., Kollman, M. S., Song, C., Shilling, J. E., and Ng, N. L.: Effects of NOx on the Volatility of Secondary Organic Aerosol from Isoprene Photooxidation, Environ. Sci. Technol., 48, 2253–2262, 2014.

Yee, L. D., Craven, J. S., Loza, C. L., Schilling, K. A., Ng, N. L., Canagaratna, M. R., Ziemann, P. J., Flagan, R. C., and Seinfeld, J. H.: Secondary organic aerosol formation from low-NO$_x$ photooxidation of dodecane: evolution of multigeneration gas-phase chemistry and aerosol composition, J. Phys. Chem. A, 116, 6211–6230, 2012.

Zaveri, R. A., Easter, R. C., Shilling, J. E., and Seinfeld, J. H.: Modeling kinetic partitioning of secondary organic aerosol and size distribution dynamics: representing effects of volatility, phase state, and particle-phase reaction, Atmos. Chem. Phys., 14, 5153–5181, doi:10.5194/acp-14-5153-2014, 2014.

Zhang, X., Pandis, S. N., and Seinfeld, J. H.: Diffusion-limited versus quasi-equilibrium aerosol growth, Aerosol Sci. Technol., 46, 874–885, 2012.

Zhao, R., Lee, A. K. Y., and Abbatt, J. P. D.: Investigation of Aqueous-Phase Photooxidation of Glyoxal and Methylglyoxal by Aerosol Chemical Ionization Mass Spectrometry: Observation of Hydroxyhydroperoxide Formation, J. Phys. Chem. A, 116, 6253–6263, 2012.

Zhou, S., Shiraiwa, M., McWhinney, R., Pöschl, U., and Abbatt, J. P. D.: Kinetic limitations in gas-particle reactions arising from slow diffusion in secondary organic aerosol, Faraday Discuss., 165, 391–406, 2013.

Ziemann, P. J. and Atkinson, R.: Kinetics, products, and mechanisms of secondary organic aerosol formation, Chem. Soc. Rev., 41, 6582–6605, 2012.

Zuend, A. and Seinfeld, J. H.: Modeling the gas-particle partitioning of secondary organic aerosol: the importance of liquid-liquid phase separation, Atmos. Chem. Phys., 12, 3857–3882, 2012, http://www.atmos-chem-phys.net/12/3857/2012/.